Automated Segmentation of Low Light Level Imagery using Poisson MAP-MRF Labelling

Hugh Gribben[1], Paul Miller[1], Hongbin Wang[1], and Mark Browne[2]

[1]The Institute of Electronics, Communications and Information Technology (ECIT)
Queen's University Belfast, Belfast, UK. BT3 9DT

[2]Andor Bioimaging Division, Morrisville, USA. NC 27560

hgribben01@qub.ac.uk

Abstract

An automated unsupervised technique, based upon a Bayesian framework, for the segmentation of low light level imagery is proposed. Primarily, Mixture Modelling is used to provide a baseline estimate. This estimate is then refined to consider spatial correlations using Markov Random Field (MRF) Modelling. The technique has been implemented assuming low-light level Poisson statistics, and the results compared to the more widely used assumption of Gaussian statistics. Investigations revealed the Poisson technique quantitatively outperforms the Gaussian technique for synthetic low light imagery, both before and after avalanche multiplication, via the multiplication register of a Low-light Level Charge Coupled Device (L3CCD). The technique was then applied to the task of segmenting a biomedical dataset obtained from a L3CCD. Qualitative results were promising, again showing improvement over the Gaussian technique.

1 Introduction

The high sensitivity of recently developed L3CCD sensors provides us with the ability to acquire multidimensional datasets at high temporal sampling rates under low-light level conditions. This allows, for the first time, the study of the dynamics of biomedical bodies such as cells, and their intra-cellular components. The novel imaging method allows vast multidimensional datasets to be regularly acquired. Novel statistical distributions are present within the data; due to both the initial low-light levels at which the data is acquired, and the avalanche multiplication to which the data is subjected via the L3CCD. Along with the size of these datasets, the statistical distributions present a new challenge to improve upon the existing methods currently in use within the area of biomedical image processing. In this work, an automated unsupervised technique, based upon the Bayesian framework and assuming low-light level statistics, is proposed for the segmentation of L3CCD imagery.

Related work in this area has included the segmentation of medical images using an automated volumetric segmentation system [1]. In this work, the authors combine techniques in the areas of statistical reasoning and multi-resolution analysis, to differentiate tissue types in brain images obtained from Magnetic Resonance Imaging (MRI) and Positron Emission Tomography (PET) imaging techniques. Similarly to Peng et. al. [2], in which a method is presented to segment 3D MRI brain images, a Spatial Gaussian Mixture Model is used to represent the intensity probability distribution of each of the brain tissues. Like the work presented here, this method consists firstly of a learning process based on the Expectation Maximisation (EM) algorithm to estimate parameters. A classification algorithm based upon the Iterated Conditional Modes (ICM) algorithm is then used to perform segmentation of the biomedical imagery; using these parameters. In both cases, the results found show an accurate method for the segmentation of the example images. Deng [3], using a similar method for unsupervised MRF modelling, has also found encouraging results. While related works [1-4] have adopted a Gaussian Maximum a Posterior-MRF (MAP-MRF) approach, we instead assume low-light level Poisson statistics for the optimisation of the novel L3CCD data; and apply the resulting technique. To the authors' knowledge, this Poisson MAP-MRF approach has not previously been applied to this class of imagery. The paper is organised as follows. In section 2, our Poisson MAP-MRF approach is defined. In section 3, results obtained are reviewed and analysed. Finally, conclusions and future work are discussed in section 4.

2 Poisson MAP-MRF Approach

2.1 Low Light Level Statistics and L3CCD Theory

At low light levels (up to approx. 50 photons per pixel per integration time), photon counts are distributed according to the Poisson distribution [5]

$$p(y \mid \mu) = \exp\left(y \log(\mu) - \mu - \log(y!)\right) \qquad (1)$$

where y is a non-negative number of occurrences, and μ the mean number of occurrences. L3CCDs contain a multiplication register which implements electron avalanche multiplication so that a large mean gain can be realised prior to the conventional readout amplifier. When the photon input level is small and the gain large, the L3CCD output can be estimated by providing the probability distribution of the L3CCD with (1), giving the joint distribution [5]

$$p(x,u) = \sum_{n=1}^{\infty} \frac{\exp\left(-\mu - \dfrac{x}{g}\right)\mu^n \left(\dfrac{x}{g}\right)^{n-1}}{g(n-1)!n!} \qquad (2)$$

This is the probability the output will be x when the mean light level is μ, with the input number of photons equal to n, and a mean gain of g.

2.2 Derivation of Poisson MAP-MRF Technique

Using Bayes estimation, a risk is minimized to obtain an optimal estimate. In terms of the segmentation problem, according to the Bayes rule, the posterior probability of a labelling estimate *X* given an observation *Y* can be computed by $P(X|Y) = P(Y|X)P(X)/P(Y)$ where *P(X)* is the prior probability of X, *P(Y/X)* is the likelihood function of *X* with respect to *Y*, and *P(Y)* is the density of *Y*. The minimal risk estimate is therefore $X^* = \arg\max_X P(X|Y)$, the MAP estimate. As *P(Y)* is a constant for fixed *Y,* the MAP estimate is equivalently found by

$$X^* = \arg\max_X \{P(Y|X)P(X)\} \tag{3}$$

In many applications, an initial estimate for *X* is obtained using mixture modelling, assuming a mixture density of Gaussian distributions. However, taking into account the Poisson nature of the low-light level imagery we wish to segment, we model the intensity distribution as a mixture of Poisson distributions, given by

$$f(Y_i \mid \theta, \lambda) = \sum_{k=1}^{K} \lambda_k f_k(Y_i \mid \theta_k) \tag{4}$$

where *K* is the number of assumed Poisson distributions, Y_i = observed value at pixel *i*, θ_k = the set of mean vectors $\{\mu_k\}$; $f_k(\cdot \mid \theta_k)$ is a Poisson density with mean μ_k; $\theta = (\theta_1, \ldots, \theta_k)$ and $\lambda = (\lambda_1, \ldots, \lambda_K)$ is a vector of mixture probabilities such that $\lambda_k \geq 0 \ (k = 1, \ldots, K)$ and $\sum_{k=1}^{K} \lambda_k = 1$ [1].

The algorithm used in practice to find the mixture of distributions that best model the dataset is the EM algorithm, first introduced by Dempster et al. [6]. This is an iterative algorithm, which estimates the parameters via a Maximum Likelihood (ML) criterion. The mixture density returned can then be used to associate pixel observations with a Poisson density *k* using a simple ML estimation

$$k^* = \arg\max_k f_k(Y_i \mid \theta_k) \tag{5}$$

A label X_i is then given to pixel *i* in the estimate *X*, corresponding to k^*.

In MAP-MRF labeling, *P(X/Y)* is the posterior distribution of a MRF. The prior model *P(X)* takes into account spatial correlations present in an image, and is dependent upon the type of scene. Assuming our scene to be a piecewise constant surface, we consider an indicator function, $I(X_i, X_j) = 1$ if $X_i = X_j$ and otherwise = 0. The Potts model can be described by $P(X) \propto \exp\left(\phi\sum_{i,j} I(Xi, Xj)\right)$, where the sum is computed over all neighbour pairs. Spatial homogeneity in the model is expressed using the parameter ϕ, small values implying randomness, and large values implying uniformity [7]. Let $N(X_i)$ be the neighbourhood of X_i, and let $U(N(X_i),k)$ be the number of neighbourhood pixels with a label corresponding to a distribution *k*. The prior energy for each distribution labelled *k* can then be defined as the negative of the sum of all the clique potentials over *X* [8]

$$E(X) = -\sum_{i \in S} \phi U(N(X_i), k) \tag{6}$$

where S is the set of pixel sites, and i the site currently under consideration.

The likelihood model $P(Y/X)$ depends upon physical considerations. With the traditional approach, Y is assumed to be a degraded version of a MRF realization X due to independent additive Gaussian noise. Taking a Gaussian distribution as a special form of a Gibbs distribution, advantage is then taken of a MRF's equivalence to a Gibb's distribution [8], to then define the likelihood as $P(Y \mid X) = \exp\left(-E(Y \mid X)\right) \Big/ \prod_{i \in S} \sqrt{2\pi\sigma_i^2}$, where σ_i^2 is the variance of the estimated Gaussian distribution at pixel i, and

$$E(Y \mid X) = \sum_{i \in S} (X_i - Y_i) \Big/ 2\sigma_i^2 \tag{7}$$

is the likelihood energy. Instead, we assume low-light statistics, taking each observed pixel value to be the output of a Poisson process. We then take (1) as a special form of the Gibbs distribution, as opposed to the Gaussian distribution. Next, we take advantage of a MRF's equivalence to a Gibb's distribution to define the likelihood as $P(Y \mid X) = \exp\left(E(Y \mid X)\right)$ where

$$E(Y \mid X) = -\sum_{i \in S} \left(Y_i \log(X_i) - X_i - \log(Y_i)\right) \tag{8}$$

is the likelihood energy. Finally, the prior and likelihood energies are added to yield the posterior energy. In the Gaussian case, this gives

$$E(X \mid Y) = \sum_{i \in S} (X_i - Y_i) \Big/ 2\sigma_i^2 - \sum_{i \in S} \phi U(N(X_i), k) \tag{9}$$

For our updated Poisson technique, we replace (9) with

$$E(X \mid Y) = -\sum_{i \in S} \left(Y_i \log(X_i) - X_i - \log(Y_i)\right) - \sum_{i \in S} \phi U(N(X_i), k) \tag{10}$$

The MAP estimate can then be found by then minimising the posterior energy. Practically, this can be performed by the use of the ICM algorithm, originally introduced by Besag [9]. This is an iterative algorithm that begins with the observed scene Y, and the initial estimate of the true scene X from mixture modelling. By considering each pixel site in turn, it then proceeds to provide a new estimate of the true scene iteratively, until convergence is reached, or a maximum number of iterations complete. The optimal value of ϕ for each iteration is chosen via Pseudo-Likelihood Information Criterion (PLIC) analysis. This is an automated Bayesian technique that considers the ratio of likelihoods of output models to determine the optimal model. In the Gaussian case, a single iteration of the ICM requires (11) for each pixel i, where μ_{kG} is the Gaussian mean of state k.

$$k^* = \arg\min_k (\mu_{kG} - Y_i) \Big/ 2\sigma^2 - \phi U(N(X_i), k) \tag{11}$$

A label X_i is then given to pixel i in the updated estimate X, corresponding to k^*. For our updated Poisson technique, we replace (11) with

$$k^* = \arg\min_k - \left(Y_i \log(\mu_{kP}) - \mu_{kP} - \log(Y_i)\right) - \phi U(N(X_i), k) \tag{12}$$

where μ_{kP} is the Poisson mean of state k.

3 Results and Analysis

3.1 Segmentation of Low-Light Data

The proposed technique was initially applied to synthetic data with mean gain set to 1 for analytical purposes. In the first case, an image is produced by the creation of a binary random pattern, by convolving a normally distributed 256x256 random array with a Gaussian filter. This allows us to quantify the spatial dependencies within the data by comparison of the Full Width at Half Maximum (FWHM) parameter of the filter used (The greater the FWHM, the greater the spatial dependencies). Pixels are then labelled depending upon value. This provides us with our "true scene" $\hat{X}$ that we wish to recreate via our segmentation technique (Fig. 1(a)). Poisson noise is then added to each pixel, the mean Poisson value being dependent upon the initial labelling, to give low-light synthetic data (Fig. 1(b)). Figs. 1(c) and 1(d) show qualitative results giving the initial estimate returned from the mixture modelling step, and the application of the MAP-MRF technique. Here, Poisson noise is added to the true scene with means equivalent to light levels of 4 and 10 photons/pixel/integration time, dependent upon the initial labelling. The application of the MAP-MRF technique shows considerable improvement over the initial estimate returned from the mixture modelling step, as well as a close approximation to the true scene we are attempting to recreate.
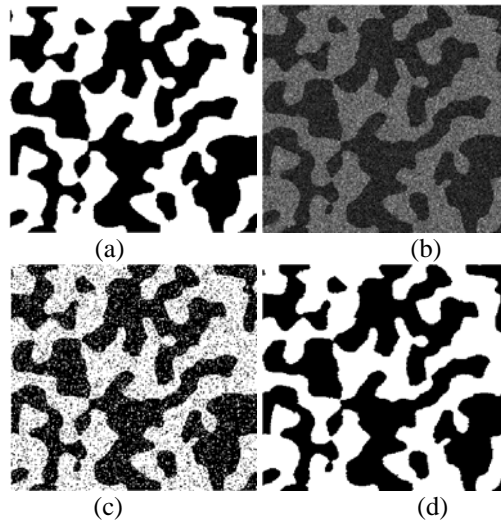

(a)

(b)

(c)

(d)

Figure 1: Automated Segmentation of Synthetic Data (a) 'True Scene' with FWHM = 11.77 (b) 'Observed Scene' (True Scene with Poisson noise added (c) Output - Mixture Modelling Segmentation of b (d) Output – Poisson MAP-MRF Segmentation of b

Fig. 2 shows quantitative results obtained from the MAP-MRF technique compared to the initial estimate returned from the mixture modelling step, as ϕ is increased over 10 iterations of the ICM algorithm for different initial true scenes with increasing spatial dependencies from 2(a) through 2(c). Segmentation was performed 10 times for each differing spatial dependency, and the average error rates calculated.
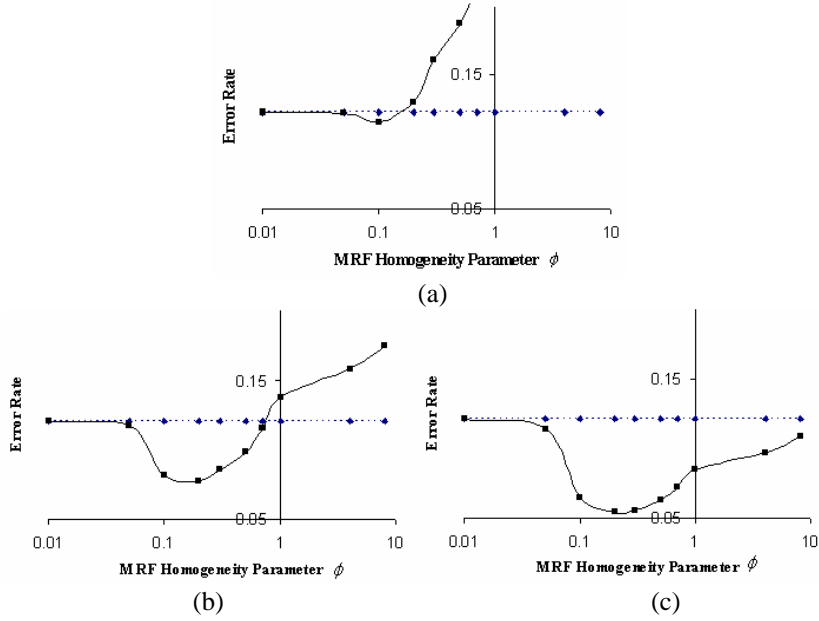

(a)

(b)   (c)

Figure 2: Output Error Rates obtained from technique over 10 iterations varying ϕ (Solid Curve) compared to output from mixture modelling alone (Dotted Curve). Data created with Poisson distributed values of 4 and 10 photons/pixel/integration time (a). FWHM = 0.47 (b) FWHM = 2.4 (c) FWHM = 5.9

Quantitative results were found by comparing returned estimates X with the true scene using the error rate $err = \sum_{i \in S} (1 - M) \Big/ S_n$,where S_n is the total number of pixels and $M =$ 1 if $X_i = \overset{\Lambda}{X}_i$, $M = 0$ otherwise. Minimisation of the error rate corresponds to the best input prediction, i.e. an ideal segmentation should give an error rate of $err = 0$.

It can be seen in each case that an optimal value for the error rate improves upon the error rate returned from mixture modelling alone. An optimal value of ϕ is shown in each case where the error rate is minimised, i.e. where the Potts model with a value of ϕ best represents the spatial dependencies present in the input image. The figures also show that as the spatial dependencies increase from 2(a) through 2(c), improvements in the corresponding results can be clearly seen. We can see that the optimal error rates returned are improved as the spatial dependencies within the original true scene are increased, and that the error rate is better than that returned with mixture modelling alone over a larger percentage of chosen ϕ. These results are intuitive with what we

would expect, and were replicated for all synthetic imagery with average light levels less than 100 photons/pixel/integration time.

Fig. 3 shows the average percentage improvement of our Poisson MAP-MRF technique over the more widely used Gaussian MAP-MRF technique in terms of optimal error rate returned. Results were obtained from averaging optimal error rates returned from both approaches with 15 different synthetic images. The figure shows that the Poisson approach outperforms the Gaussian approach as the average light level decreases. This follows intuitively, from our earlier investigation of low-light level statistics.
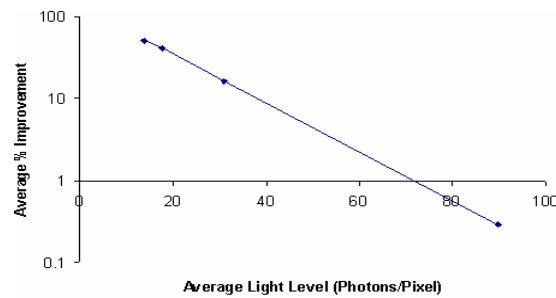

Figure 3: Average % Improvement with Poisson MAP-MRF over Gaussian MAP-MRF as a function of average light level for low-light level Synthetic Imagery

3.3 Segmentation of L3CCD Imagery

Synthetic imagery was then created to approximate the output from a L3CCD sensor with varying mean gains. This was achieved by replicating the avalanche multiplication process applied by the multiplication register of a L3CCD on the low light synthetic imagery.

Fig. 4 shows the average percentage improvement of the Poisson MAP-MRF technique over the Gaussian MAP-MRF technique in terms of optimal error rate returned; with differing mean gains applied.
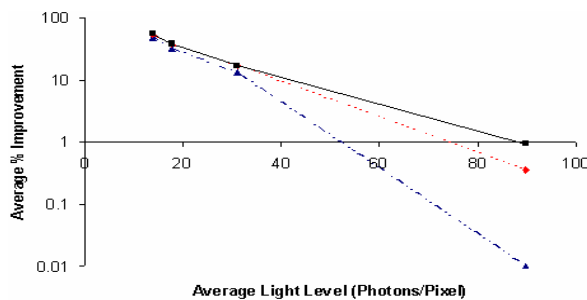

Figure 4: Average % Improvement with Poisson MAP-MRF over Gaussian MAP-MRF as a function of average light level for Synthetic L3CCD Imagery created with varying mean gains of 100 (Solid Curve), 500 (Dotted Curve), and 700 (Dash-Dotted Curve).

The figure again clearly shows that the Poisson approach outperforms the Gaussian approach for all mean gains shown, improving as the average light level decreases. We can also see that, in general, as the mean gain increases, the percentage improvement decreases somewhat due to the fact the distributions present in the data tend to Gaussian as the gain increases.

Finally, the technique has been applied to the segmentation of data obtained from a L3CCD sensor. The 3D dataset of dimension 208*235*100 used for these results consists of Green Fluorescent Protein labelled telomeres in a cell nucleus; acquired via a L3CCD sensor. These are a component of cells which act as a buffer at the end of chromosomes to prevent the loss of genetic information needed to sustain its activities; with implications in anti-aging and anti-cancer therapy [10]. The technique was also applied to a Poisson distributed PET imaging source, of dimension 128*128*35 for comparison; as the technique is applicable to any Poisson distributed dataset. The phantom data used was an oval shaped object containing six fillable spheres of variable diameters filled with fluorodeoxyglucose. Both datasets are shown in Fig. 5.
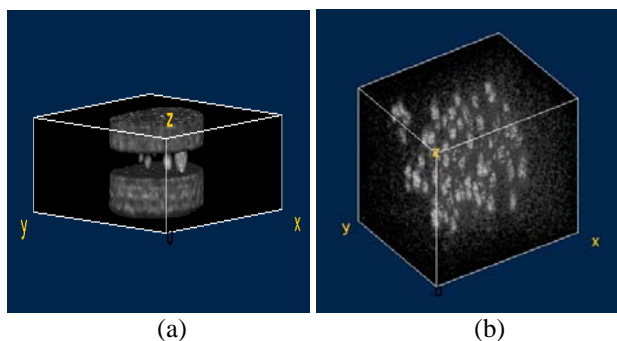

(a)   (b)
Figure 5: (a) 3D PET Dataset (b) 3D L3CCD Dataset

Table 1 shows the error rate obtained from various segmentation techniques applied to both datasets, as compared to manual segmentation.

	Otsu (Automated Thresholding) [*10e-3]	Gaussian MAP-MRF [*10e-3]	Sq-Root Gaussian MAP-MRF [*10e-3]	Gaussian MAP-MRF with Median Filter [*10e-3]	Poisson MAP-MRF [*10e-3]
PET Imagery	199	0.653	178	0.687	0.357
L3CCD Imagery	849	1.30	1.10	1.20	0.614

Table 1: Error Rates obtained from various Segmentation Techniques as compared to Manual Segmentation

In each automated MAP-MRF case, the number of total components in an image was chosen via Bayesian Information Criterion (BIC) analysis (3 in each case for the L3CCD data), and the value of ϕ chosen via PLIC analysis. Like PLIC, BIC is an

automated Bayesian technique that considers the ratio of likelihoods of output models to determine the optimal model. Included are the Otsu automated thresholding technique [11], the Gaussian MAP-MRF technique, the Gaussian MAP-MRF technique applied to the square-root values of the original dataset, and with a median filter applied; and the Poisson MAP-MRF technique.

The results clearly show that the Poisson MAP-MRF technique provides a result closer to that obtained via the manual segmentation technique than the Otsu and Gaussian MAP-MRF techniques in both cases. The Poisson MAP-MRF technique also results in less noisy isolated pixels, and clearer isolated telomere bodies than the corresponding Gaussian results for the L3CCD data, as shown in the qualitative results of Fig. 6. The reason for this is that assuming Poisson statistics allows us to better model the true distributions present in the L3CCD datasets.
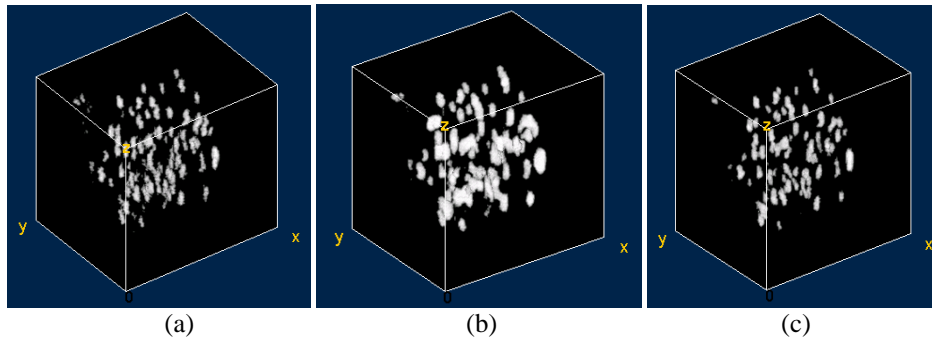

(a)   (b)   (c)

Figure 6: Segmentation of L3CCD Dataset (a) Output From Manual Technique (b) Output from Gaussian MAP-MRF Technique (c) Output from Poisson MAP-MRF Technique

Both fully-automated techniques gave comparable computational times of approximately 60 secs per ICM iteration for a 14-bit image of dimension 208x235; using a 2800Mhz x86 GenuineIntel processor. To conclude, better qualitative segmentation was found with the Poisson technique over the Gaussian using a fully automatic technique, with comparable processing times.

4 Conclusions and Future Work

We have presented a novel technique, using a Poisson MAP-MRF approach for the segmentation of low-light imagery which, to our knowledge, has not previously been applied to the described classes of imagery. We have shown that the technique provides improvement over a simple mixture modelling approach, and that improved results are seen as the spatial dependencies within the data are increased. The technique shows improvement over a Gaussian MAP-MRF approach at low light levels, and has been applied to real L3CCD data, with successful results. Future work shall include further investigations to take fuller advantage of the distributions present within L3CCD datasets. Application of the technique to 4D imagery shall be implemented.

Acknowledgements

References

[1] D. Montgomery, A. Amira, & F. Murtagh, "An automated volumetric segmentation system combining multi-scale and statistical reasoning," *Proceedings of the IEEE International Symposium on Circuits and Systems, Kobe, Japan*, 4, pp. 3789-3792, May 2005.

[2] Z. Peng, W. Wee & J. Lee, "MR brain imaging segmentation based on spatial Gaussian Mixture Model and Markov Random Field,*" IEEE International Conference on Image Processing*, 2005.

[3] H. Deng & D.A. Clausi, "Unsupervised Image Segmentation Using A Simple MRF Model with A New Implementation Scheme", In *Pattern Recognition, 2004. ICPR 2004. Proceedings of the 17th International Conference on*, 2, pp. 691-694, IEEE, August 2004.

[4] J. Goldberger & H. Greenspan, "Context-based segmentation of image sequences," *IEEE Transactions on Pattern Analysis and Machine Intelligence,* 28(3), March 2006.

[5] G. Basden, C. A. Haniff & C. D. Mackay, "Photon counting strategies with low-light level CCDs," *Mon. Not. R. Astron. Soc,* 345, pp. 985-991, 2003.

[6] A. Dempster, N. Laird, & D. Rubin, "Maximum likelihood from incomplete data via the EM algorithm," *Journal of the Royal Statistical Society*, 39(1), pp. 1-38, 1977.

[7] D. Stanford & A. E. Raferty, "Approximate Bayes factors for image segmentation: The pseudo-likelihood information criterion (PLIC*)," IEEE Transactions on Pattern Analysis and Machine Intelligence*, 24(11), November 2002.

[8] S. Z. Li, *Markov Random Field Modelling in Computer Vision* New York: Springer-Verlag, 2001.

[9] J. Besag, "On the statistical analysis of dirty pictures," *Journal of the Royal Statistical Society, Series B (Methodological)*, 48(3), pp. 259-302, 1996.

[10] Y. Cong, W. E. Wright, & J. W. Shay, "Human telomerase and its regulation," *Microbiology Molecular Biology Review*, 66(3), pp. 407-425, September 2002.

[11] N. Otsu, "A Threshold Selection Method from Gray-Level Histograms," *IEEE Transactions on Systems, Man, and Cybernetics*, 9(1), pp. 62-66, 1979.